PNAS RESEARCH ARTICLE | NEUROSCIENCE OPEN ACCESS

Synaptophysin chaperones the assembly of 12 SNAREpins under each ready-release vesicle

Manindra Bera[a,b], Abhijith Radhakrishnan[a,b,1], Jeff Coleman[a,b,1], R. Venkat K. Sundaram[a,b], Sathish Ramakrishnan[a,c], Frederic Pincet[a,b,d], and James E. Rothman[a,b,2]

Contributed by James E. Rothman; received July 6, 2023; accepted September 19, 2023; reviewed by Axel T. Brunger and Thomas H. Soellner

The synaptic vesicle protein Synaptophysin (Syp) has long been known to form a complex with the Vesicle associated soluble N-ethylmaleimide sensitive fusion protein attachment receptor (v-SNARE) Vesicle associated membrane protein (VAMP), but a more specific molecular function or mechanism of action in exocytosis has been lacking because gene knockouts have minimal effects. Utilizing fully defined reconstitution and single-molecule measurements, we now report that Syp functions as a chaperone that determines the number of SNAREpins assembling between a ready-release vesicle and its target membrane bilayer. Specifically, Syp directs the assembly of 12 ± 1 SNAREpins under each docked vesicle, even in the face of an excess of SNARE proteins. The SNAREpins assemble in successive waves of 6 ± 1 and 5 ± 2 SNAREpins, respectively, tightly linked to oligomerization of and binding to the vesicle Ca^{++} sensor Synaptotagmin. Templating of 12 SNAREpins by Syp is likely the direct result of its hexamer structure and its binding of VAMP2 dimers, both of which we demonstrate in detergent extracts and lipid bilayers.

neurotransmitter release | synaptophysin | Synaptotagmin1 | VAMP2 | SNAREpins

Significance

Synaptophysin (Syp) is the most abundant protein of synaptic vesicles (SVs), yet it has an unknown function. Here, we establish that Syp forms a hexameric complex sequestering ~12 copies of the VAMP2. These v-SNAREs assemble into SNAREpins in two equal waves organized by oligomerization of the Synaptotagmin as ready-release vesicles are formed in vitro. In the absence of Syp, two waves are also observed, but the number of SNAREpins in each varies widely. We suggest that a single Syp hexamer in each vesicle symmetrically organizes six pairs of peripheral and central SNAREpins, the latter being directly bound to the Synaptotagmin ring. This gives rise to the symmetrical ring-like arrangement of densities observed by cryo-EM tomography under each SV.

Although the total free energy available from folding up ("zippering") of the SNARE complex is ~70 k_BT (1), most of this exceptionally large amount of energy is utilized before bilayer fusion in order to irreversibly force two docked membranes into close proximity. This can leave as little as ~5 k_BT (2) available from terminal zippering to overcome the ~30 k_BT energy barrier (3, 4) for bilayer fusion. Therefore, to achieve the ultrafast fusion required by synaptic vesicles (SVs), multiple SNAREpins must be simultaneously released for terminal zippering. Because they are mechanically coupled by attachment to locally rigid bilayers, as few as 3 to 6 SNAREpins can potentially cooperate to trigger fusion pore opening in <1 ms (5).

The surprising finding from cryoelectron tomography that each such SV sits atop a sixfold symmetric ring-like arrangement of protein densities (6, 7) implied that there are 6 (or potentially a multiple of 6) SNAREpins beneath each ready-release vesicle. The ring likely contains the Ca^{++} sensor Synaptotagmin, as the isolated protein self-assembles into similar size rings (8) and mutation of Synaptotagmin disorganizes the densities under the SVs (9). Munc13, a chaperone needed for SNAREpin assembly at synapses (10–13), capable of self-assembly into hexagons between phospholipid bilayers (14) provides one possible mechanism to template up to 6 SNAREpins at a time (15).

The abundant SV-specific protein Synaptophysin (Syp) could provide a second independent mechanism for templating a multiple of 6 SNAREpins. It has long been known that Syp binds the SV v-SNARE VAMP (16–18). Betz et al. (19) and more recently Stowell and colleagues have reported from averaged negatively stained EM images that purified Syp can exist as a hexamer in cholesterol-containing detergent solution (20) where it binds the synaptic v-SNARE VAMP2 in an approximately 1:2 molar ratio (21). This implies that a Syp hexamer could theoretically sequester up to 12 copies of VAMP, offering a simple mechanism that could assemble 12 SNAREpins per vesicle (22). However, direct evidence for this hypothetical complex has been lacking.

Why is such a basic fact as the number of SNAREpins that are assembled in a ready-release SV still unknown three decades after the SNARE complex was identified and implicated in neurotransmitter release (23–27)? The explanation is that despite enormous advances in imaging technologies, there are still no suitable methods with sufficient sensitivity and resolution to detect and quantify individual molecular components of the release machinery at synapses in situ. For example, a careful study of the SNARE assembly chaperone Munc13 using single molecule-based super-resolution imaging could reliably detect approximately 5 to 10 copies of Munc13 associated with each ready-release vesicle at the neuromuscular junction but could not quantify their number more precisely (28).

To gain further insights, it is necessary to utilize reconstituted cell-free systems that reproduce ultrafast fusion (29, 30), and which are compatible with well-established single-molecule methods that enable straightforward counting of directly labeled proteins

Author contributions: M.B., A.R., S.R., F.P., and J.E.R. designed research; M.B., A.R., J.C., and R.V.K.S. performed research; M.B., A.R., S.R., and F.P. analyzed data; and M.B., A.R., J.C., F.P., and J.E.R. wrote the paper.

Reviewers: A.T.B., Stanford University; and T.H.S., University of Heidelberg.

The authors declare no competing interest.

[1]A.R. and J.C. contributed equally to this work.

[2]To whom correspondence may be addressed. Email: james.rothman@yale.edu.

This article contains supporting information online at https://www.pnas.org/lookup/suppl/doi:10.1073/pnas.2311484120/-/DCSupplemental.

Published October 30, 2023.

in buffers and geometries that favor signal detection over backgrounds. Total reconstitution of ultrafast release minimally requires the synaptic SNAREs, the Ca^{++}-sensor Synaptotagmin, the lipid PIP_2 (phosphatidylinositol 4, 5-bisphosphate) (for Synaptotagmin function), and Complexin and has been achieved both between vesicles in suspension (31, 32) and between single-vesicle and planar suspended bilayers (30, 33–35). In these systems, the plasma membrane SNAREs Syntaxin and SNAP25 are preassembled into t-SNAREs, thereby bypassing the requirement for the specialized chaperoned Munc13 and its partner Munc18 (36, 37). The ultrafast synchronous release is also reconstituted in a complete system in which SNARE assembly is chaperone-dependent (12, 38).

We recently described a further advance upon the vesicle-suspended bilayer system in which the bilayer is now held within ~5 mm of a coverslip above a buffer whose refractive index is raised with a polymer (Iodixanol) to match that of the glass. This chip geometry enables total internal reflection fluorescence (TIRF) microscopy, whose sensitivity enables the quantitation of single molecules associated with individual docked vesicles whose fate can be followed after the addition of Ca^{++} (39).

In this report, we utilize this advance to directly test the idea that Syp can determine the number of SNAREpins assembling between a ready-release vesicle and its target membrane bilayer. In order to isolate this potential mechanism from the alternative templating mechanism involving Munc13, we utilized the chaperone-free system involving preassembled t-SNAREs. We begin by first using related single molecule methods to directly establish the subunit structure of Syp and its complex with the v-SNARE VAMP2, both in lipid bilayers and in detergent solution.

Results

Syp Forms Hexameric Clusters Containing up to 12 Copies of VAMP2 in Lipid Bilayers. To test for the formation of oligomeric complexes of Syp and VAMP2 in the native environment of a phospholipid bilayer, we labeled these proteins with different colored dyes, reconstituted them into a common supported lipid bilayer, and determined whether they bound each other and if so in what numerical combinations. By counting single molecules at a very low surface density (~10 Syp molecules per ~1 μm^2), we could exclude associations by coincidence despite the limits of optical resolution. We chose supported bilayers because the lateral diffusion of proteins is very slow due to absorption to the glass (40, 41), facilitating cluster analysis.

Therefore, recombinant Halo-tagged Syp was expressed in HEK293 cells, purified from detergent extracts using its 12-his-tag (*SI Appendix*, Fig. S1*C*), and labeled with Alexa488 chloroalkane. Recombinant VAMP2 (mutated from wild-type by S28C and C103A to allow for selective labeling with Alexa647-maleimide), was expressed in *E. coli* and purified according to its 6-his tag (29, 30, 34). These proteins were then co-reconstituted (*SI Appendix*, Fig. S1*C*) in a mole ratio of ~4 VAMP2 per Syp into small unilamellar vesicles (SUVs) containing phospholipids with 20 mol% cholesterol, included because cholesterol promotes VAMP-Syp association (21, 42, 43). The SUVs were then applied to a clean glass coverslip with 5 mM $MgCl_2$ to form supported bilayers (44, 45) and then imaged by TIRF microscopy sequentially with 488-nm (Syp) and 647-nm (VAMP2) lasers. We quantified cluster sizes from both the intensity values and step photobleaching curves.

Syp considered by itself (Fig. 1 *B*, *Top*) existed in clusters containing 6 ± 2 copies per cluster. When Syp molecules co-clustering with VAMP2 were considered separately, these Syp clusters (Fig. 1 *B*, *Middle*) contained an indistinguishable 6 ± 1 copies of Syp per cluster and now also contained 11 ± 3 copies of VAMP2 (Fig. 1 *B*, *Bottom*). Under these conditions ~50% of VAMP2 is co-clustered with Syp, the balance being unbound and free.

VAMP2-Dependent Assembly of Syp into Single Hexameric Particles in Solution. From the previous experiment, we can conclude that Syp efficiently forms hexamers in phospholipid bilayers, each of which efficiently sequesters up to ~12 copies of VAMP2, even when these proteins are very sparse. For comparison, the average surface concentrations of VAMP2 and Syp are about 100 and 10 monomers per μm^2, respectively, as compared to the ~9,000 and ~4,000 molecules/μm^2 that can be calculated for native SVs from published data (46).

These considerations suggest that complexes between VAMP2 and Syp may also exist in a dilute detergent solution to allow independent single-molecule measurements of stoichiometry following adsorption to cover slips from a dilute solution. Using 1 μM Alexa488-Halo-Syp resulted in clusters containing an average of 3 ± 1 copies (Fig. 2 *A*, *Top*). Incubation with unlabeled VAMP2 (4 μM final concentration) produced larger Syp oligomers, now averaging 5 ± 2 copies each (Fig. 2 *A*, *Middle*).

This difference suggested that hexamers of Syp not only bind VAMP2 but are also stabilized by VAMP2 binding. If so, sequestering VAMP2 should destabilize the Syp oligomers. This can be achieved by adding soluble t-SNAREs (the 1:1 complex of the cytoplasmic domain of Syntaxin1 and SNAP25) to form SNARE complexes with the VAMP2, and these can be further stabilized by Complexin. This is exactly what happens (Fig. 2 *A*, *Bottom*). Now Syp is almost completely dissociated to 2 ± 1 copies, i.e., to monomers.

To independently determine the stoichiometry of VAMP2 binding to Syp in a detergent solution supplemented with 0.1% cholesterol, we used even lower concentrations of Syp-Halo488 (100 nM) to favor dissociation into monomers and also added VAMP2 (400 nM, now labeled with Alexa647). We monitored both molecules coming together at the same spot simultaneously with 100 ms time resolution (Fig. 2*B*). Under these conditions, we can not only rule out coincidental binding but also determine the stoichiometry of this complex directly with a small number of photobleaching steps.

As anticipated, the vast majority of Syp molecules (90 ± 5%) were now only monomers and only 10 ± 5% of these were in a complex with VAMP2. Each such monomer of Syp contained either one (Fig. 2 *B*, *Top*) or two copies of VAMP2 (Fig. 2 *B*, *Bottom*) but never more than 2 copies. The ratio of Syp_1Vamp_1:Syp_1Vamp_2 in this population of complexes was ~2:1. Given the concentrations of VAMP2 and Syp in this experiment (400 nM and 100 nM), respectively, and assuming a simple two-step independent binding model where $[Syp] + 2[VAMP] \rightarrow [Syp_1VAMP_1] + [VAMP] \rightarrow [Syp_1VAMP_2]$, then the unitary binding constant will be in the range of 1 to 100 μM in the detergent solution.

We conclude that each subunit of Syp can separately bind up to 2 copies of VAMP2 and that a hexamer of Syp in cholesterol-containing lipid bilayers should bind up to 12 copies of VAMP2, in agreement with the measurements using lipid bilayers.

Single-Particle Cryo-EM of the Native Syp-VAMP2 Complex. Native Syp-VAMP2 complex was purified from rat brains using a previously described protocol (21). The purity of this complex was established with sodium dodecyl sulfate–polyacrylamide gel electrophoresis (SDS-PAGE) (*SI Appendix*, Fig. S3*A*) and its components were confirmed by western blotting (*SI Appendix*, Fig. S3*B*). The ratio of VAMP2 to Syp was 1.7 ± 0.2 moles/mole based on the amount of Coomassie staining relative to subunit

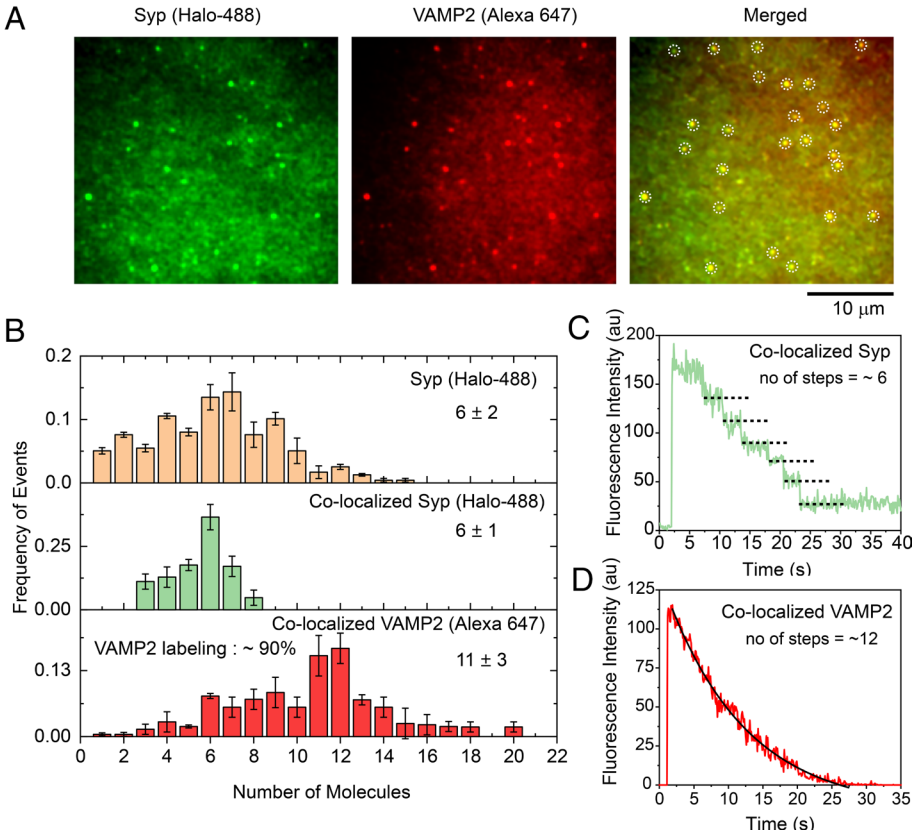

Fig. 1. $(Syp)_6$-$(VAMP2)_{12}$ complex formation on supported bilayers. Syp-Halo (Alexa 488) and VAMP2 (Alexa 647) are incorporated into the 20% cholesterol–containing small SUVs to form a supported bilayer onto a glass slide. (*A*) Syp and VAMP2 imaged with 488- and 633-nm lasers, respectively, with TIRF microscopy show distinct clusters. Colocalized clusters are marked with a white dashed circle. (The scale bar is 10 μm.) (*B*) Histograms for Syp (orange), colocalized with VAMP2 (green) and VAMP2 colocalized with Syp (red). Mean ± SEM values of all Syp (6 ± 2), colocalized Syp (6 ± 1), and colocalized VAMP2 (11 ± 3) cluster size distributions are indicated on the right side of each panel. Black error bars denote the SDs. The total no of particles (n) for all Syp and both colocalized clusters are 1,953 and 381, respectively. All the clusters are calculated from three independent experiments. Both Syp-Halo 488 and VAMP2-Alexa 647 labeling percentages were ~95% and ~90%, respectively. (*C* and *D*) Examples of step photobleaching curves for colocalized Syp (6 distinct steps shown using black dotted lines) and colocalized VAMP2 (total steps ~12) are presented in *C* and *D*, respectively. VAMP2 bleaching steps are fitted with an exponential decay equation (black solid line). The fitted initial intensity, i.e., the prefactor of the fit, is used to derive the total no of steps.

molecular masses (*SI Appendix*, Fig. S3*A*). The freshly purified samples were applied to grids and were frozen before being imaged by 200-kV Glacios (*SI Appendix*, Fig. S3*C*). A total of 731 movies were collected during a single session and the images were analyzed using RELION 3.1 (47). A template-free autopicking procedure was used for autopicking, which yielded a dataset of 635,143 particles. Several rounds of reference-free two-dimensional (2D) classifications were carried out to remove bad particles. Individual 2D classes of the final set of homogenous particles frequently revealed molecules with clear evidence of 6 subunits (*SI Appendix*, Fig. S3*D*) as implied by the biochemical analysis (Figs. 1 and 2) and as previously suggested by negative-stained images (19, 20). We believe that these 2D classes represent a Syp hexamer containing unit that can template 12 SNAREpins. Further processing of these selected set of particles (~70,000 particles) yielded 3D density maps with very low resolution which we decided not to pursue. The poor quality of the density maps is possibly due to a combination of reasons such as the presence of a strong detergent micelle of Triton X-100 covering the protein complex, the difficulty in aligning the particles due to the absence of strong cytoplasmic densities for alignment, preferential orientation (lack of side views) as wells as the innate conformational heterogeneity of the purified Syp-VAMP2 complex in solution. Extensive studies of the protein complex reconstituted in nondetergent platforms are required for elucidating a high-resolution structure and revealing the interaction between Syp and VAMP2.

Counting SNAREpins on Docked Vesicles. To measure the number of SNAREpins associated with each docked vesicle, we take advantage of the fact that Complexin binds tightly with very low nM affinity to the SNARE complex in 1:1 stoichiometry via its central helix (48–51). In particular, the central helix binds to partially zippered SNARE complexes containing only VAMP2 residues 29 to 60 (52–54). Therefore, Complexin is expected to bind to half-zippered SNAREpins (52). As with ready-release vesicles in vivo, cell-free reconstitutions are clamped beyond this residue (55, 56); thus, we can count clamped SNAREpins simply by counting the number of bound Complexin molecules.

To fluorescently label Complexin1 (*SI Appendix*, Fig. S2 *A* and *B*), we utilize its sole cysteine (residue number 105) which is near the C terminus domain and is uninvolved in binding to VAMP2 and Syntaxin in the SNARE complex (48, 54). This Cys is labeled with maleimide-conjugated Alexa647, a measured efficiency ranging from ~50 to 85% (moles/mole) over numerous preparations (*Materials and Methods*).

When the labeling efficiency is high (~85%) and there are small numbers (<7) of SNAREpins on a vesicle, discrete steps of quantal photobleaching are reliably observed and counted (see Fig. 3*B* for examples). On the other hand, when larger numbers of (>6) SNAREpins are present, discrete step-wise photobleaching is rarely observed (Fig. 3*C*). In this case, the number of fluorescent dye molecules can be measured indirectly and less precisely from the prefactor of the exponential decay curve fitting, and considering

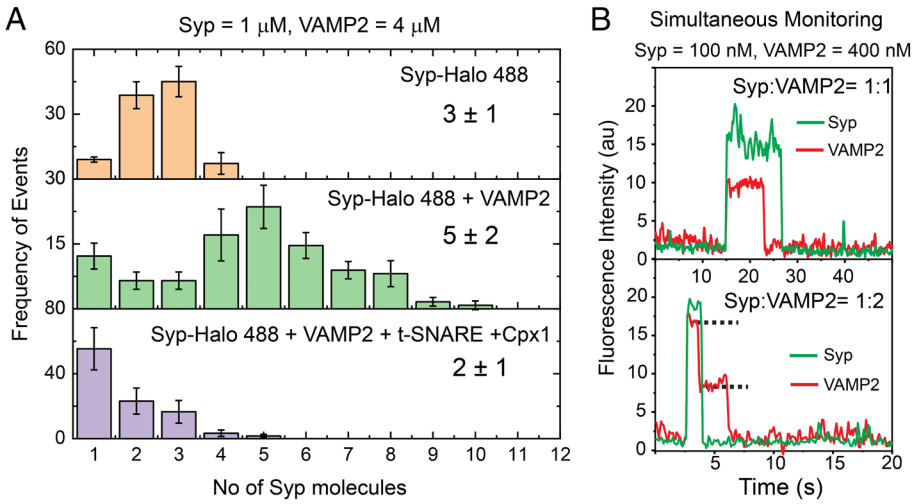

Fig. 2. VAMP2-dependent Syp_6 assembly and the 2:1 complex in solution. (*A*) Distribution of copy numbers of Syp (Alexa-488) particles when incubated alone (1st panel in orange), after overnight incubation with VAMP2 (1:4 molar ratio, 2nd panel in green), and after a second incubation with t-SNAREs and Complexin (2 μM each) for 30 min at RT (3rd panel in purple). Each protein sample was briefly exposed onto a freshly BSA-coated glass slide and washed with fresh buffer before imaging with a 488-nm laser. Incubation with VAMP2 shifted the Syp stoichiometry from 3 ± 1 to 5 ± 2. Adding t-SNAREs and Complexin reduced the stoichiometry down to 2 ± 1. n > 721 for each case, N = 3, and the error bars represent the SD of the means. (*B*) Time-dependence fluorescence intensity of Syp (Alexa 488, ~95% labeling efficiency) and VAMP2 647 (Alexa 647, 90% labeling efficiency) complexes after O/N incubation at 1:4 molar ratio and deposition onto a glass slide and monitored simultaneously with 488 and 647 nm lasers. Only particles with the simultaneous landing of Syp and VAMP2 were considered actual Syp/VAMP2 complexes. Both panels show one example of a 1:1 (*Upper*) and 1:2 (*Lower*) Syp: VAMP2 complex. The black dashed line denotes the number of steps for VAMP2. The sudden rise in fluorescence intensity at 15 s (*Top*) and 2.5 s (*Bottom*) corresponds to the landing of the complexes.

average unit fluorophore intensity as measured from single bleaching steps observed in vesicles with low copy numbers in the vicinity (Fig. 3*C*, see *Materials and Methods* for details).

To add precision when measuring larger numbers of SNAREpins, we utilized defined mixtures of extensively labeled (~85%) and label-free Complexins produced to achieve partial (25% or 50%) labeling. To illustrate why this is useful, consider a case where there are 12 SNAREpins. This vesicle will bind 12 Complexins. If only 25% bear the dye, then on average every such vesicle will have 3 dye molecules, a small number that can be reliably counted by photobleaching (Fig. 4 *D*, *Left* panel). However, the actual number will differ from vesicle to vesicle. Some individual vesicles will have bound (at random) 4 dyes and 8 dye-free Complexins; others 2 dyes and 10 dye-free Complexins, and so on. The distribution of labeled complexin follows a binomial distribution with a probability equal to the labeled fraction. Hence, the raw discrete step data for 25%, 50%, or undiluted samples (Fig. 3 *D* and *E*) can be fitted by a binomial distribution to calculate the average number of SNAREpins for the entire vesicle population more accurately than would have been possible from total intensity analysis. The variation of the mean for the fraction of labeled Complexin follows a straight line with an intercept at 0 and a slope corresponding to 12 ± 1 SNAREpin per vesicle (Fig. 3*F*).

We performed several controls to further establish the specificity of the Complexin signal for counting SNAREpins. As expected, the Complexin fluorescence signal is only detected on the suspended bilayer portion of the chip where it is associated with VAMP2-containing SUVs docked to t-SNARE-containing suspended bilayers (*SI Appendix*, Fig. S2*C*) and is not observed when vesicles lack the v-SNARE and are instead docked by Synaptotagmin1 (*SI Appendix*, Fig. S2*D*). This also indirectly rules out the possibility that the labeled Complexin binds to docked vesicles via its curvature-sensing C-terminal amphipathic helix (57, 58) to a detectable extent when diluted for single-molecule studies under our conditions. This was directly established by deleting the amphipathic helix (Complexin1 residues 26 to 83; *SI Appendix*, Fig. S5). Using this probe and the linear fitting of the mean values (*SI Appendix*, Fig. S5*D*) we measured 11 ± 2 SNAREpins per vesicle, indistinguishable from the 12 ± 1 measured under the same conditions using the standard full-length Complexin probe (Fig. 4 *B*, *Top*). These controls, together with the nature of the results obtained, validate the sensitivity and specificity of the methods we employ to count SNAREpins.

Syp Limits the Number of SNAREpins to Twelve. Based on the robust observation of a $VAMP_{12}$-Syp_6 complex in lipid bilayers (Fig. 1) and the frequent observation of discrete $VAMP_{1\text{-}2}$-Syp_1 subcomplexes in dilute solution (Fig. 2), we hypothesize that the 12 copies of VAMP2 bound to Syp in vesicles will be kinetically advantaged in forming SNAREpins with t-SNARE-containing bilayers. Such a structure, involving 12 SNAREpins, a Syp hexamer, and potentially numerous copies of Syt, would occupy most or all of the interface between the vesicle and bilayer, excluding other SNAREpins from forming. Therefore, our hypothesis predicts that in the absence of Syp, there will be a variable number of SNAREpins, but adding Syp will standardize the number to (theoretically) 12.

We first measured the number of SNAREpins in vesicles lacking Syp (Fig. 4*A*) but containing variable (5 to 60) average numbers of externally oriented VAMP2 and ~22 (on average) copies of externally oriented Syt and labeled Complexin mixtures. In all of these compositions, vesicles are known from previous work to be efficiently clamped and synchronously released (<13 ms) when Ca^{++} is added (29, 34). With low (5 or 10) copies of external VAMP2, the ready-release vesicles had 6 ± 1 and 7 ± 1 SNAREpins on average, respectively (Fig. 4 *A*, *Top* two panels). With high (25 or 60) copies of external VAMP2, the ready-release vesicles had now had 19 ± 6 (Mean ± SEM) and 23 ± 4 SNAREpins on average, respectively (Fig. 4 *A*, *Bottom* two panels), but the numbers in individual cases are highly variable and can even exceed ~30 SNAREpins per vesicle. These cases seem mainly to involve larger vesicles in the population (*SI Appendix*, Fig. S7) and likely correspond to cases where there are extensive contact surfaces (as distinct from a discrete point of contact) between docked vesicles observed by Cryo-electron microscopy (cryo-EM) (6, 7). For comparison, native SVs contain about 70 copies of VAMP2, ~30 copies of Syp (46), and ~15 to 20 copies of Syt1 (46, 59).

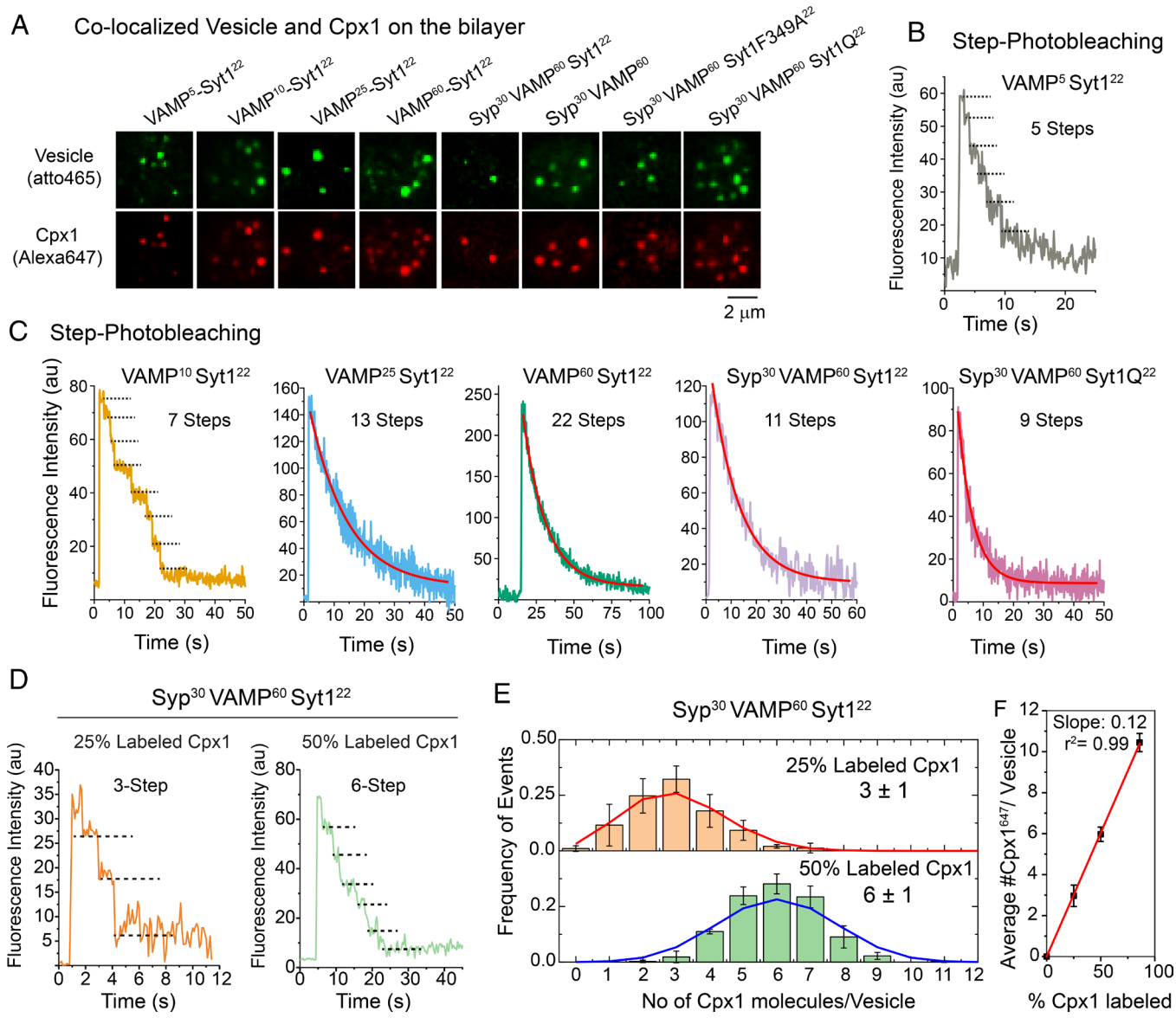

Fig. 3. SNAREpin counting under a docked vesicle. (*A*) Representative images for the colocalized docked vesicle and Cpx1 signal on the bilayer. Vesicle and Complexin were, respectively, labeled with Atto 465 DOPE lipid and Alexa 647-maleimide (85% labeling efficiency). Vesicles and Cpx1 were incubated for 5 min, washed three times, and imaged with 488-nm laser and 633-nm laser with 100 ms acquisition time. (Scale bar, 2 μm.) (*B* and *C*) Representative traces for Cpx1 photobleaching curves. Cpx1 signals under VAMP2^{5}Syt1^{22} (gray) and VAMP2^{10}Syt1^{22} (yellow) vesicles displayed 5 and ~7 distinguishable photobleaching steps, respectively. However, the Cpx1 signal under VAMP2^{25}Syt1^{22}, VAMP2^{60}Syt1^{22}, VAMP2^{60}Syp^{30}Syt1^{22}, and VAMP2^{60}Syp^{30}Syt1Q^{22} vesicles showed smoothly decaying photobleaching curves, indicating higher numbers of photobleaching steps. All the curves were fitted with exponential decay curve fitting to obtain the number of labeled Cpx1 (see the *Materials and Methods* section). (*D*) Examples of step bleaching curves of VAMP2^{60}Syp^{30}Syt1^{22} vesicles, clamped in the presence of 2 μM Cpx1 with 25% (*Left*) and 50% (*Right*) labeling efficiency. ~3 and ~6 photobleaching steps were observed with 25% and 50% labeled Cpx1, respectively. (*E*) Distributions of the labeled Cpx1 per vesicle. All the 25% (*Top*) and 50% (*Bottom*) labeled Cpx1 numbers were binned from 0 to 12 with bin size 1 and plotted as histograms. Red and blue curves represent the predicted binomial distribution keeping dye labeling at 25% and 50%, respectively, and the final SNAREpin number kept at 12. Mean ± SEM values at corresponding labeling efficiency are shown inside the graph. (*F*) The average numbers of labeled Cpx1 per vesicle are plotted with Cpx1 labeling percentages and fitted linearly keeping the intercept at 0. Error bars are SDs. For a description of the 85% labeled Cpx1, see Fig. 5*B*. Slope and linear regression (r^2) were calculated to be 0.12 and 0.99, respectively. For each case, n >150, N >3.

When the native Syp-VAMP2 complex purified from rat brains (~30 copies of Syp per vesicle and ~60 copies of VAMP2) was added during reconstitution, the results were dramatic. Now only 12 ± 1 SNAREpins were assembled (Fig. 4 *B*, *Top*), compared with the exceptionally broad distribution ranging from 5 to 35 in the absence of Syp (Fig. 4 *A*, *Bottom*). Syp limited the number of SNAREpins to 12 ± 2 even in the absence of Syt (Fig. 4*B*, 2nd from top). We also introduced recombinantly purified Syp (~30 copies per vesicle) from HEK 293 cells and supplemented with recombinant VAMP2 (from *E.coli;* ~60 copies per vesicle). We observed similar results with a slightly broader distribution.

Importantly, when Syt1 was introduced, the result was a very narrow distribution that closely fits the predicted binomial distribution for 12 SNAREpins considering the experimental dye labeling efficiency of 85% (*SI Appendix*, Fig. S4). When Syt1 was present, but could not bind SNAREpins (due to mutations in its primary binding site; Fig. 4*B*, 3rd panel, Syt1Q), or could not assemble ring oligomers (due to an F349A mutation; Fig. 4 *B*, *Bottom* panel), SNAREpin templating by Syp was largely unaffected (12 ± 2 and 13 ± 1 SNAREpins per vesicle, respectively); however, distributions were broadened significantly. In control experiments, we confirmed that including Syp (30 copies) in the

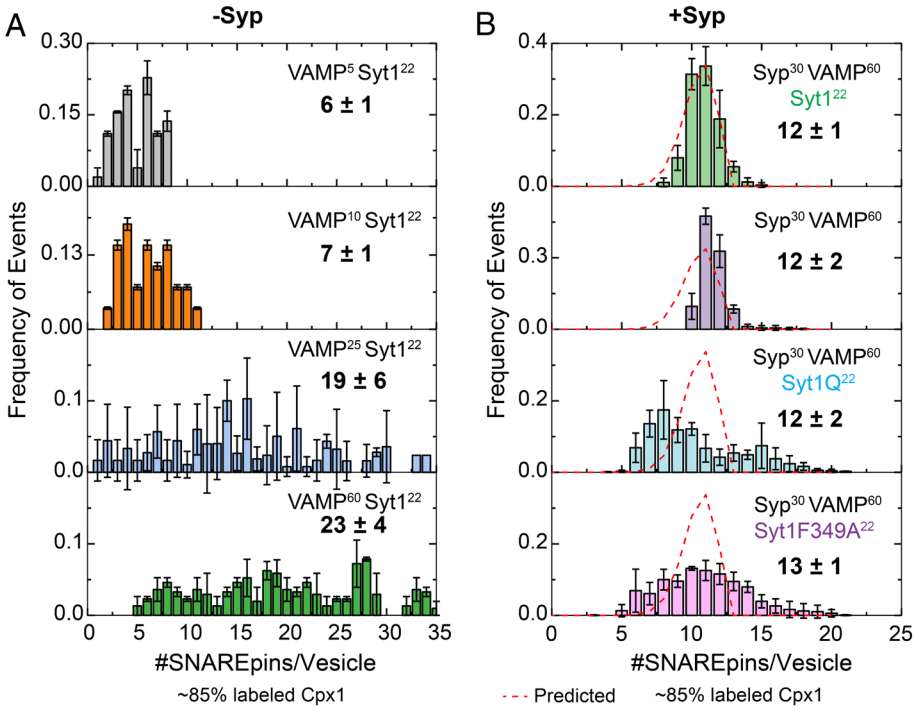

Fig. 4. Syp templates 12 SNAREpins. (*A*) Distribution of the copy numbers of Cpx1 colocalized with docked vesicles without Syp. The total number of Cpx1 molecules under each docked vesicle was calculated from photobleaching steps or total intensity distributions and plotted as frequency histograms with one bin size. Without Syp, an increasing copy number of VAMP2 in the vesicle produces an increasing number of Complexin signals (i.e., SNAREpins). Recombinantly purified VAMP2 and Syt1 were used to reconstitute the vesicles. n > 250, N > 3 for each case. (*B*) Distribution of the copy number of Cpx1 colocalized with docked vesicles with Syp. With Syp, every vesicle tends to produce ~12 SNAREpins under each vesicle. For Syp^{30} $VAMP^{60}$ $Syt1^{22}$ (green) and Syp^{30} $VAMP^{60}$ (purple) vesicles (n > 150, N = 3 for each case), natively purified Syp-VAMP complex and recombinantly purified Syt1 (first case) were used. For the other two cases (Syp^{30} $VAMP^{60}$ $Syt1Q^{22}$ and Syp^{30} $VAMP^{60}$ $Syt1F349A^{22}$), Syp purified from HEK293 cell and recombinant VAMP2 and Syt1 were used. The red curve denotes the predicted binomial distribution of the final 12 SNAREpins while the dye labeling percentage was matched with our experimental labeling efficiency (85%). All values in bold letters denote the SNAREpin numbers (average ± SEM) for the corresponding histogram. n > 350, N > 3 for each case.

vesicles along with VAMP2 (60 copies) and Syt (22 copies) did not compromise clamping by Complexin (*SI Appendix*, Fig. S6*A*) or synchronous release (*SI Appendix*, Fig. S6 *C* and *D*). Interestingly, Complexin-dependent clamping was observed even in the absence of Syt as long as Syp was present (*SI Appendix*, Fig. S6*A*). However, Ca^{++}-dependent release from this (Complexin plus Syp) clamped state did not occur in the absence of the Ca^{++}-sensor Syt.

Biphasic SNAREpin Assembly by Syp. To study the kinetics of assembly of the 12 SNAREpins templated by Syp we continuously monitored the appearance of immobilized docked vesicles (Atto465) and SNAREpin formation (Complexin-647). Vesicles can be docked by Syt binding to PIP_2 in the suspended bilayer and/or by the first SNAREpin to form. Therefore, the vesicle always appears before or together with the Complexin fluorescence. Unexpectedly, we observed that the 12 SNAREpins form in two very distinct phases (Fig. 5*A*). In the first phase 6 ± 1 SNAREpins are rapidly assembled. Then, following a variable lag phase, a second rapid wave of assembly occurs, resulting in an additional 5 ± 2 SNAREpins. In other words, half the SNAREpins assemble right away, and the other half assemble after a prolonged delay, which averages a highly variable 0.5 ± 1 s (*SI Appendix*, Fig. S9*D*). Unlike the variable lag phase, the SNAREpins assemble at indistinguishable and rapid rates in the first (34 ± 21 SNAREpins/s) and second phases (30 ± 21 SNAREpins/s), corresponding to about 30 ms per SNAREpin.

The basis of the two phases of SNAREpin assembly seems to be in Synaptotagmin, and in particular to binding of SNAREpins to the simultaneously assembling ring of Synaptotagmin. Omitting Syt but retaining Syp produces ~12 SNAREpins, but they now assemble rapidly in a single phase (Fig. 5*B*). Replacing Syt with a mutant that does not bind SNAREpins (Syt1Q) has the same effect (Fig. 5*C*). Abolishing the ring organization but not SNAREpin binding (Syt1F349A) also eliminates the lag phase but now also greatly slows the rate of SNAREpin assembly (Fig. 5*D*). Introducing tripartite mutant in Syt1 has a little effect in the total number of SNAREpins; however, it produced wide variations in the SNAREpin assembly kinetics (*SI Appendix*, Fig. S10). Finally, the two phases of SNARE assembly are even observed in the absence of Syp, but now templating to a limit of 12 SNAREpins is lost (*SI Appendix*, Figs. S8 and S9). In the absence of Syp, the first phase produces an average of 10 ± 5 SNAREpins, and the second phase has an average of 10 ± 6 SNAREpins for a total of 21 ± 9 SNAREpins (*SI Appendix*, Fig. S9*D*).

Discussion

The simplest explanation of our observations regarding the biphasic assembly of SNAREpins is that Syp limits the number of SNAREpins to 12 and Syt ring assembly orchestrates the kinetics. The first 6 SNAREpins assemble around the Syp hexamer while binding 6 individual molecules of Syt. This assembly sterically prevents further SNAREpin assembly until additional copies of free Syt join in to assemble an organized ring containing these "central" SNAREpins. Only when this has been accomplished (during what we observe as the lag phase) can a second set of "peripheral" SNAREpins assemble in the space available outside the ring. When ring assembly is impaired, the lag phase is indefinitely extended and slower untemplated SNAREpin assembly continues as if Syp were absent. When the binding of SNAREpins to Syt is prevented, Syt no longer sterically interferes with the assembly of more than 6 SNAREpins, and the lag phase is abolished but templating to 12 SNAREpins by Syp remains.

Because each vertex of the presumably symmetric Syp hexamer presents 2 copies of VAMP2, it is evident that each copy must be

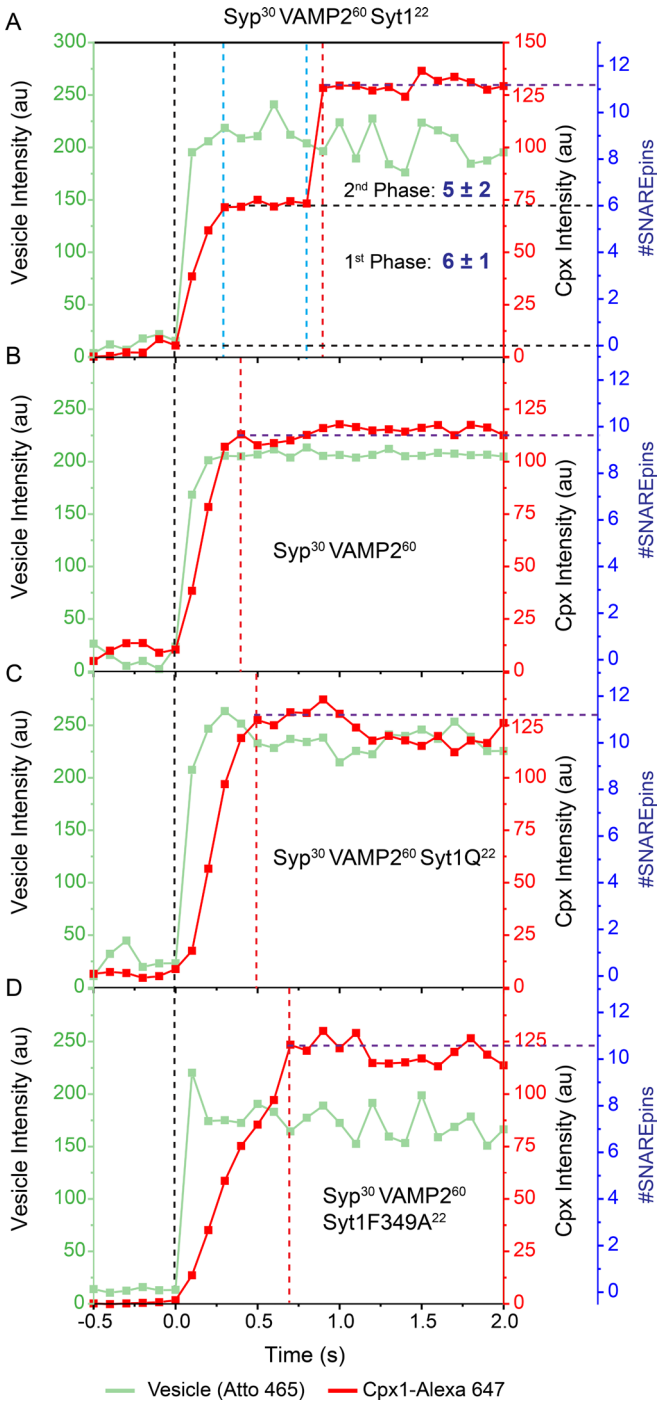

Fig. 5. Rates of SNAREpin assembly. (*A*) A representative trace for Syp^{30}VAMP2^{60}Syt1^{22} vesicles (light green) and Cpx1 (red) assembly are shown. Vesicles and Cpx1 were monitored simultaneously with 488-nm and 633-nm lasers with 100 ms acquisition time. When vesicles dock on the membrane, the Cpx1 signal starts increasing. The time point was adjusted to 0 when vesicles were docked on the membrane, represented by a vertical black dotted line. For these vesicles, Cpx1 showed a two-step assembly. Initially, it increases (1st phase, vertical black and blue dotted line) and completely stops (lag phase, two vertical blue dotted lines) and then increases again (2nd phase, vertical blue and red dotted lines). The left green axis, right red axis, and blue axis denote vesicle, Cpx1 signal, and the number of SNAREpin formations, respectively. The number of SNAREpins formation (blue axis) was calculated from the increase in the Cpx1 signal (right red axis). Black horizontal dotted lines represent the start and end of 1st phase assembly, respectively. The magenta horizontal dotted line marks the end of the assembly. (*B*) Syp^{30}VAMP2^{60} vesicle showed a one-step rapid Cpx1 assembly. Syp^{30}VAMP2^{60}Syt1Q^{22} (*C*) and Syp^{30}VAMP2^{60}Syt1F349A^{22} (*D*) vesicles also showed one-step rapid and slow Cpx1 assembly, respectively. Vertical black and horizontal magenta dotted lines in all panels denote the vesicle arrival and end of SNAREpin assembly, respectively.

bound differently, either directly to Syp or indirectly as a VAMP2 dimer (21). In either case, their unequal geometries would be expected to afford one copy more reactivity toward t-SNAREs than the other. An alpha-fold prediction of what this structure could look like is shown in *SI Appendix*, Fig. S11 *A–E*. Interestingly, one VAMP2 transmembrane domain (TMD) is predicted to interact directly with Syp 1st and 4th TMD ("inner" VAMP2), and the second VAMP2 ("outer" VAMP2) interacts only indirectly when its TMD dimerizes with the TMD of the first VAMP2. We suggest that one copy of Syp at each vertex is predetermined to assemble the central SNAREpin onto Syt and its ring, while the other (slower-reacting) VAMP2 is destined to form a peripheral SNAREpin. It would seem natural to assume the outer VAMP2 forms the peripheral SNAREpin while the inner VAMP2 assembles into the central SNAREpin. However, alpha-fold offers other types of predictions where one VAMP2 binds to similar to earlier "inner VAMP2" and other VAMP2 binds to the opposite of the Syp (*SI Appendix*, Fig. S11 *F* and *G*).

In essence, each Syp would asymmetrically bind a VAMP2 dimer. Depending on the stability of the VAMP2 dimers and the stability of Syp oligomers, a mixture of Syp_1 monomers, Syp_1VAMP_1 and Syp_1VAMP_2 species would predominate in dilute solution at one extreme, whereas homogeneous $VAMP_{12}Syp_6$ 18-mers would assemble at high concentrations in lipid bilayers, matching our observations. Moreover, VAMP2 is known to dimerize in cholesterol-containing detergent solutions (43, 60) although not in lipid bilayers as an isolated protein (61, 62) and indirect evidence suggests that it interacts with the 3rd and 4th TMD helices of Syp (21, 63).

We have separately suggested that each peripheral (64) SNAREpin is further linked by a bridging molecule of Complexin to the central SNAREpin with which it shares a common Syp vertex to add an energy boost ("turbocharging") to accelerate fusion pore opening and expansion (64). We have previously provided evidence that central and peripheral SNAREpins (produced in the absence of Syp) are thus linked in this trans-clamping arrangement in which the Complexin accessory helix from one SNAREpin binds to the zippering end of a second SNAREpin (29). The hallmark of trans-clamping is the requirement for an intact accessory helix, also required to stabilize vesicles in the Syp-containing vesicles with 12 SNAREpins (*SI Appendix*, Fig. S12).

It is unclear in our experiments whether the peripheral SNAREpins assemble in the first wave followed by the central SNAREpins or vice versa. In any case, the order may differ when t-SNAREs are artificially preassembled vs. when all three synaptic SNAREs are co-assembled by the chaperones Munc13 and Munc18 (12, 65). In particular, the autoinhibited Munc13 lateral hexamer is expected to occupy the same space as the Syt ring and is expected to be required for central SNAREpin assembly (14), leading to the prediction (64) that peripheral SNAREpins may assemble before central SNAREpins when the Munc chaperones and Syt are both present.

Syp has long been known to form a complex with VAMP2 in extracts from synaptosomes (16, 18), but a more specific molecular function or mechanism of action of Syp in exocytosis has been lacking. This is because knockouts of Syp genes in mice have minimal effects on exocytosis (66) as distinct from SV recycling by endocytosis (67, 68). Even a quadruple knockout of the Syp1 and Syp2 along with its homologs Synaptogyrin 1 and 3 had minimal effect in neuronal exocytosis (66). Our results, from a fully defined cell-free system, stand in bold contrast. Here, Syp has the remarkable and well-defined property of templating exactly 12 SNAREpins under each vesicle. This molecular mechanism is the direct result of its hexamer structure (19–21) and the stoichiometry of VAMP2 binding (21), which we have now directly established to occur in phospholipid bilayers.

To rationalize this clear mechanism of action with Syp's apparent lack of physiological importance, we need to assume that there are independent mechanisms that can adequately control the number of SNAREpins. Munc13 (cooperating with Munc18) chaperone SNAREpin assembly, and in particular, Munc13 can assemble between bilayers into at least two hexagonal oligomers (14), lateral hexagons (composed of 6 copies), and a hexamer of upright trimers (composed of 18 copies). It is possible that homeostasis can be maintained by Munc13 alone under many circumstances.

Materials and Methods

Materials. The following cDNA constructs were used in this study: full-length VAMP2 (VAMP2-His^6, residues 1 to 116); full-length $VAMP2^{4\times}$ (VAMP2-His^6, residues 1 to 116 with L70D, A74R, A81D, L84D mutations), full-length t-SNARE complex (mouse His^6-SNAP25B, residues 1 to 206 and rat Syntaxin1A, residues 1 to 288); Synaptotagmin (rat Synaptotagmin1-His^5, residues 57 to 421); and Complexin (mouse His^6-Complexin 1, residues 1 to 134). All mutants including $Syt1^{F349A}$ (F349A); $Syt1^{Q}$ (R281A/E295A/Y338W/R398A/R399A); were generated as described previously (24, 29, 34). Mouse complexin 26 to 83 was modified with a C-terminal Cys using site-directed mutagenesis. Lipids, 1,2-dioleoyl-sn-glycero-3-(phospho-L-serine) (DOPS), 1,2-dioleoyl -glycerol-3-phosphocholine (DOPC), 1,2-dipalmitoyl-sn -glycero-3-phosphoethanolamine-N-(7-nitro-2-1,3-benzoxadiazol-4-yl), PIP_2, and cholesterol were purchased from Avanti Polar Lipids (Alabaster, AL). ATTO647N-DOPE and ATTO465 DOPE were purchased from ATTO-TEC, GmbH (Siegen, Germany). Alexa maleimide 647 C2 and Alexa $Fluor^R$ 488 Halo ligand were purchased from Thermo Fisher Scientific (Waltham, MA) and Promega Madison, USA), respectively.

Protein Expression and Purification. v- and t-SNAREs, Cpx, Syt1 recombinant proteins were expressed and purified as described previously (24, 29, 69). The mouse Syp gene was cloned as a BamHI/NotI fragment into a modified pCMV6-AN-His vector (Origene, USA) that contains an N-terminal 12×His tag followed by a PreScission cleavage site. The plasmid was used to transfect Expi293F cells (Thermo Fisher, USA) following the manufacturer's protocol. Briefly, 1 μg of DNA per 1 mL of cell culture was mixed in a 1:2.5 ratio of DNA: ExpiFectamine reagent for 20 min at RT and then added to approximately 2.5×10^6 cells with >95% viability. Cells were grown at 37 °C under 8% CO2 with orbital shaking for 2 d without enhancers. The cells were centrifuged at 200 × g for 10 min, washed with Phosphate-buffered saline (PBS), and flash frozen. Harvested pellets were stored at −80 °C until needed. Expi293F cell pellets (from 50 mL of culture) were thawed and resuspended in 8 mL of 0.25 × PBS with protease inhibitors (Roche, Indianapolis, USA). Cells were lysed using a Dounce homogenizer on ice and then centrifuged in a Beckman SW55 rotor at 100,000 × g for 45 min. The pellet was resuspended in 5 mM NaH_2PO_4 (pH 6.8), 0.25% cholesterol (Avanti; Ovine Catalog # 700000P), and protease inhibitors. Triton X-100 was added to a final volume of 0.5% (v/v) and incubated on ice for 2 h with occasional inversion. The lysate was centrifuged at 45,000 × g for 30 min to pellet the insoluble fraction, and solubilized protein was incubated with 0.125 μL of HisPur Ni-NTA resin (Thermo Fisher, USA) at 4 °C overnight on a rotating wheel. The next day, the resin was washed multiple times with 20 mM NaH_2PO_4 (pH 6.8), 0.5% Triton X-100, 0.05% cholesterol, and 40 mM sucrose. Protein was eluted using the same buffer with 500 mM Imidazole (pH 6.8).

SV Preparation. SVs were purified from Sprague Dawley rat brains as described previously (70). Briefly, four rat brains were homogenized in an ice-cold buffer solution (4 mM 4-(2-hydroxyethyl)-1-piperazineethanesulfonic acid) (HEPES), pH 7.4, and 320 mM sucrose). The homogenate was centrifuged at 1,000g for 10 min at 4 °C. The pellet was removed, and the resulting supernatant was centrifuged at 15,000g for 15 min at 4 °C. The supernatant was collected and stored at 4 °C while the pellet containing synaptosomes was resuspended in the homogenization buffer and was diluted tenfold with ice-cold ddH_2O and homogenized thoroughly. The lysate was centrifuged at 17,000 g for 15 min at 4 °C. The pellet was discarded, and the resulting supernatant was combined with the supernatant from the previous step and centrifuged at 48,000 g for 25 min at 4 °C. The supernatant was further centrifuged at 300,000 g for 2 h at 4 °C, and the pellet containing SVs was collected. The SVs were immediately resuspended in 3 mL of 5 mM sodium phosphate (pH = 6.8), supplemented with 1 mM phenylmethylsulfonyl fluoride (PMSF), 1 μg/mL Pepstatin A and snap frozen in liquid nitrogen and stored in −80 °C until further use.

Purification of Native Syp-VAMP2 Complex. The Syp-VAMP2 complex was purified from SVs as described previously (21). Briefly, SVs purified from four rat brains were solubilized for 45 min at 4 °C (at 5 mg/mL) in 5 mM sodium phosphate (pH = 6.8) buffer supplemented with 1 mM PMSF, 1 μg/mL Pepstatin A, 0.2% Triton X-100, 1% cholesterol, and protease inhibitor cocktail (Roche). The solubilized Triton X-100 extract was centrifuged at 142,000 g for 45 min at 4 °C. The supernatant was applied to a dry hydroxyapatite/celite (2:1 w/w) column and was eluted with 20 mL of 5 mM sodium phosphate (pH = 6.8), 0.2% Triton X-100, 0.1% cholesterol, 1 mM PMSF, 1 μg/mL Pepstatin A, and protease inhibitor cocktail (Roche, USA). The first five fractions of the flow-through were collected as 1 mL fractions and the rest were collected as 2 mL fractions. A Coomassie gel was run to determine the purity of the Syp-VAMP2 complex in the collected fractions (*SI Appendix*, Fig. S1*A*). The Syp-VAMP2-containing fractions were then pooled and concentrated to 2 mg/mL at 4,200 g and 4 °C using 4-mL Amicon Ultra 100-kDa molecular weight cutoff centrifugal filters. The purified protein was stored at 4 °C and was immediately used for cryo-EM sample preparation and reconstitution into liposomes. The purified protein was analyzed by western blot using monoclonal Syp1 (Synaptic Systems, Germany) and monoclonal VAMP2 (Abcam, USA) antibodies to confirm the presence of the Syp-VAMP2 complex (Fig. 1*A*).

Cryo-EM Grid Preparation. 2.5 μL of freshly purified Syp-VAMP2 complex (1.5 mg/mL) was applied to C-flat-1.2/1.3-2C-T copper grids that had been glow discharged for 10 s in Argon/Oxygen atmosphere using a Solarus plasma cleaner (Gatan, Inc.). The grids were blotted for 2 s with a blot force of −1 at 4 °C under 100% humidity and were flash-frozen in liquid ethane using a FEI Vitrobot Mark IV (FEI). The grids were stored in liquid nitrogen until data acquisition.

Cryo-EM Data Acquisition and Processing. The frozen-hydrated samples were loaded on the 200-kV Glacios (Thermo Fisher Scientific) with a K2 Summit direct electron detector (Gatan, Inc.). The micrographs were collected in super-resolution mode operated using SerialEM (Version 3) software (71). A total of 731 movies were acquired at a nominal magnification of 36,000× with a physical pixel size of 1.143 Å on the specimen level. The movies were dose fractionated into 40 frames of 0.25 s each at a dose rate of 5.8 electrons/$Å^2$/s for a total dose of 58 $e^-/Å^2$ over a defocus range between −0.9 μm and −2.0 μm. The image processing was done using RELION 3.1 (47). All the 731 micrographs were motion-corrected and dose-weighted using MotionCor2 (72) with a binning factor of 2 and divided into 5 × 5 patches. The contrast transfer function was calculated with CTFFIND-4.1 (73). A template-free autopicking procedure based on Laplacian-of-Gaussian filter was used for autopicking, which yielded a dataset of 635,143 particles. Several rounds of 2D classifications using a mask of 70 Å diameter were carried out to remove bad particles and obtain a final set of homogenous particles.

Liposome Preparation. t-SNAREs and VAMP2 + Syt1 were reconstituted into SUVs using rapid detergent (1% Octyl glucoside) dilution and dialysis method as described previously (24, 29, 34, 35). The lipid composition was ~82 (mole)% DOPC, 15% DOPS, 3% PIP_2, and 0.1% ATTO465-PE for t-SNARE SUV and 88% DOPC, 10% PS, and 2% ATTO647-PE for VAMP2 and Syt1 SUVs. We used several different lipid: protein ratios in order to reconstitute to desired copy numbers (outward facing) of individual proteins. The copy number of outside-facing proteins was determined using our previously well-established method (29, 34, 35). Recombinant Syp and VAMP2 (± Syt1) were reconstituted into 50 μL of 3 mM lipids [68% (mole) DOPC, 10% DOPS, 20% cholesterol, and 2% ATTO465] that had previously been dried down to a film in a glass test tube using nitrogen gas and then stored under a vacuum for 1 h to remove any residual chloroform. Lipids were resuspended in protein and buffer (25 mM HEPES, pH 7.4, 400 mM KCl, 1 mM DTT, and 0.5% Triton X-100) up to a final volume of 100 μL and then passed through a detergent removal spin column (Pierce, catalog #87777) following the manufacturer's protocol. Volume was increased to 150 μL and dialyzed against 25 mM HEPES, 120 mM KCl, and 1 mM DTT overnight to remove any residual detergent. The next day, 150 μL of 80% Nycodenz (in the same buffer) was mixed with the sample and then loaded into a 0.8-mL tube (Beckman Coulter, catalog #344090), overlaid with 250 μL of 30% Nycodenz, followed by 50 μL of HEPES buffer. Tubes were centrifuged in an SW55 rotor at 48,000 rpm for 4 h. Proteoliposomes were collected from the gradient near the buffer/30% Nycodenz interface. Native Syp-VAMP2 complex was also reconstituted following the same protocol except no extra VAMP2 was supplied. Protein reconstitution efficiency was routinely checked with SDS-PAGE and Coomassie staining (*SI Appendix*, Fig. S1). Based on the densitometry analysis of

Coomassie-stained SDS gels, the copy number of each protein per vesicle was estimated from trypsin digestion and Coomassie blue staining as described previously.

Stoichiometry of Syp and VAMP2 on Supported Bilayers. To measure the stoichiometry of the Syp-VAMP2 complex on a supported bilayer, 1 mM (total) SUVs [60 (mole)% DOPC, 15% DOPS, 5% DOPE-PEG 2000, and 20% cholesterol] were dried with N_2 gas and kept under vacuum for another 2 to 4 h. Dried lipid was dissolved with 25 mM HEPES, pH 7.4, 150 mM KCl, 0.2 mM tris(2-carboxyethyl)phosphine (TCEP), and 2% Triton X-100. Prelabeled and purified Syp-Halo (Alexa 488) and VAMP2 (Alexa 647) proteins were added into the mixture with a protein: lipid ratio of 1:20,000 and 1:5,000, respectively. 100 mg prewashed Bio-beads SM2 (Bio-Rad, Hercules, CA) were incubated with that mixture for another 30 min at room temperature with gentle shaking. The liposomes were dialyzed overnight with a 6 to 8 kD cutoff against a detergent-free HEPES buffer. The liposomes were floated up with a discontinuous gradient of Opti prep. Samples were collected from the top carefully avoiding any Opti prep contamination and further dialyzed for another 2 h at 4 °C. The supported bilayer was created by Mg^{2+} (5 mM) induced bursting of the liposomes in ibidi glass-bottom chambers (ibidi GmbH, Germany). The bilayer was extensively washed with HEPES buffer. The bilayer was imaged with a TIRF (Nikon) microscope using 488- and 633-nm lasers. Photobleaching of the protein cluster was analyzed with Image J.

Syp-VAMP2 Counting on a Glass Surface. Recombinantly purified and labeled Syp-halo 488 (1 μM) was mixed with unlabeled VAMP2 at a 1:4 molar ratio overnight at 4 °C in a buffer containing 5 mM NaH_2PO_4, pH 6.8, 50 mM KCl, 0.2% Triton X-100, 0.2 mM TCEP, and 0.1% cholesterol. A 5-μL sample was spotted very briefly onto a freshly BSA-coated glass bottom dish (MatTek Corporation, Ashland, MA) and then quickly washed with excess buffer. Syp-halo 488 was imaged with TIRF (Nikon) using a 488-nm laser. The same overnight mixture was further supplemented with 2 μM preassembled t-SNAREs and Complexin. After 30-min incubation at room temperature, a similar method was applied to count Syp again. For dual monitoring, both Syp-Halo 488 (1 μM) and VAMP2 Alexa 647 (4 μM) labeled proteins were incubated overnight at 4 °C in a buffer consisting of 5 mM Na_2HPO_4, pH 6.8, 50 mM KCl, 0.2% Triton X-100, 0.2 mM TCEP, and 0.1% cholesterol. The mixture was diluted (10×) with the same buffer and quickly spotted on the glass bottom dish (BSA coated). Both proteins were monitored using 488- and 647-nm lasers with dual viewer 2 equipped in Nikon TIRF.

Single Vesicle Docking, Clamping, and Fusion Assay. All the single-vesicle fusion measurements were carried out with suspended lipid bilayers as previously described (29, 30, 35). Complexin at a final concentration of 2 mM was added before the addition of vesicles when required. Vesicles (100 nM lipids) were added from the top and monitored for 10 min using a 641-nm laser. We employed ATTO647-PE fluorescence to track vesicle clamping and fusion events. Fusion (lipid mixing) was attested by monitoring a burst and then a rapid decrease in fluorescence intensity as the lipid diffuses away. The fate of each vesicle was monitored and plotted as a "survival curve" which represents the fraction of vesicles that docked to the planar bilayer and proceed to spontaneous fusion or immobile docked. After the initial 10-min interaction phase, 100 mM $CaCl_2$ was added from the top to monitor the effect of Ca^{2+} on the docked vesicles. Again, the vesicle survivals of the immobile docked vesicles were analyzed, and fractions were binned with 147 ms time. Calcium was monitored as with Ca^{2+}- sensor Calcium Green conjugated to a lipophilic 24-carbon alkyl chain (Calcium Green C24) introduced in the suspended bilayer to directly monitor the arrival of Ca^{2+}. Details of this method were described in our earlier work. The fusion probability was calculated at the end of 2 min incubation. All experiments were performed at 37 °C using an inverted laser scanning confocal microscope (Leica-SP5) equipped with a multiwavelength argon laser including 488, diode lasers (532 and 641 nm), and a long-working distance 40X water immersion objective (NA 1.1).

Protein Labeling. Purified complexin proteins ($Cpx1^{1-134}$ and $Cpx1^{26-83}$-Cys) and VAMP2 (S28C, C103A) were incubated overnight with Alexa maleimide 647 C2 dye (Thermo Fisher Scientific Cat No: A20347) with a 1:5 molar ratio in the presence of 5% Dimethylsulfoxide (DMSO). Syp-Halo protein was incubated with 5 times molar excess halo ligand Alexa 488 (Promega, USA) overnight at 4 °C. Excess dye was removed twice using the dye removal column (Thermo Scientific, Cat No 22858), and then, protein was loaded into Superdex 200 and concentrated using Amicon Ultra-4 (3K cutoff, Merck). The labeling percentage was calculated according to the manufacturer's protocol. Protein concentration was checked with Bradford assay and dye concentration was measured from the absorbance (Alexa 647 at 651 nm and Alexa 488 at 494 nm), and labeling efficiency was calculated with three repeats.

Complexin Counting and Rate of SNARE Assembly Measurement. All the complexin counting experiments underneath docked vesicles were performed with TIRF (Nikon) on a reconstituted planar suspended bilayer on the silicon surface. The method to create a suspended bilayer compatible with single-molecule imaging was described in detail elsewhere (39). Briefly, t-SNARE-containing giant unilamellar vesicles (~82% DOPC, 15% DOPS, 3% PIP_2, and 0.1% Atto 465-DOPE) were prepared using the osmotic shock protocol and burst onto freshly plasma-cleaned Si/SiO2 chips containing 5-μm-diameter holes in the presence of HEPES buffer (25 mM HEPES, 140 mM KCl, and 1 mM DTT) supplemented with index matching 45% Optiprep(™) (STEMCELL Technologies) and 5 mM $MgCl_2$. After waiting 20 min, the suspended bilayer was extensively washed with HEPES buffer containing 1 mM $MgCl_2$. Before adding any vesicles, the bilayer was completely bleached, and then, 2 μM total complexin (with corresponding labeled protein) was added and mixed well. Then, 100 nM SUVs (63% DOPC, 15% DOPS, 20% cholesterol, and 2% Atto 465-DOPE) containing different proteins were added and monitored both vesicle and complexin simultaneously with 488- and 633-nm solid-state laser, respectively, using dual viewer 2. To generate more statistics on the vesicle and complexin counts, excess complexin was removed by washing three times with HEPES buffer. Both vesicle and complexin were imaged, and complexin signals were subjected to photobleaching using a 633-nm laser with 100 ms acquisition time. All the data were analyzed with ImageJ. The number of complexin signals underneath a vesicle was calculated from the steps of the photobleaching curves. However, we could not precisely determine the number of steps when the number of molecules was higher than 5 to 7. The photobleaching curves were fitted with an exponential decay curve with Eq. **1**.

$$I(t) = I_0 e^{\frac{-t}{\tau}} + B, \quad [\mathbf{1}]$$

Where I(t) denotes the intensity at time t, I_0 is the initial intensity before bleaching, τ is the time constant, and B is the background. Hence, the copy number, N can be obtained from Eq. **2**.

$$N = \frac{I_0}{i}, \quad [\mathbf{2}]$$

Where i is the average unit intensity of a single fluorophore as determined from the small clusters. For rate of assembly, vesicle and corresponding complexin signal were plotted to monitor the SNAREpin formation. Realtime SNAREpin formation was calculated from the complexin signal using Eq. **3**.

$$f_{SNAREpin}(t) = (I_{Cpx}(t) - B) * I_p / i. \quad [\mathbf{3}]$$

$I_{Cpx}(t)$ represents the complexin intensity at time = t, B = background intensity, I_p =labeling percentage factor, and i, average intensity for one complexin molecule. All the complexin counting data were converted to histograms with 1 bin size. The prediction was calculated using a binomial distribution. We assume that there are exactly N_S SNAREpins that form in the contact between the vesicle (Syp^{30} $VAMP2^{60}$ $Syt1^{22}$) and the membrane and that a single Cpx binds to each SNAREpin. Only a fraction f of the Cpx molecules is labeled. Since Cpx binds randomly to SNAREpins, the number of fluorescent dyes, n, follows a binomial distribution:

$$p(n) = \binom{N_S}{n} f^n \left(1-f\right)^{N_S-n}. \quad [\mathbf{4}]$$

Using N_S = 12 and the three labeling fractions used, approximately 0.25, 0.5, and 0.85, the dye copy number distributions can be directly predicted and compared with the experimental ones.

Data, Materials, and Software Availability. All study data are included in the article and/or *SI Appendix*.

ACKNOWLEDGMENTS. We thank Dr. Kirill Grushin for helping in cryo-EM data collection and processing and generating the structural models. We also thank Dr. Seong Lee for his help in isolating rat brains.

Author affiliations: [a]Nanobiology Institute, Yale University School of Medicine, New Haven, CT 06520; [b]Department of Cell Biology, Yale University School of Medicine, New Haven, CT 06520; [c]Department of Pathology, Yale University School of Medicine, New Haven, CT 06520; and [d]Laboratoire de Physique Statistique, Ecole Normale Supérieure, Paris Sciences et Lettres Research University, CNRS, Sorbonne Université, Université de Paris Cité, 75005 Paris, France

1. Y. Zhang, Energetics, kinetics, and pathway of SNARE folding and assembly revealed by optical tweezers. *Protein Sci.* **26**, 1252–1265 (2017).
2. Y. Gao *et al.*, Single reconstituted neuronal SNARE complexes zipper in three distinct stages. *Science* **337**, 1340–1343 (2012).
3. R. J. Ryham, T. S. Klotz, L. Yao, F. S. Cohen, Calculating transition energy barriers and characterizing activation states for steps of fusion. *Biophys. J.* **110**, 1110–1124 (2016).
4. C. Francois-Martin, J. E. Rothman, F. Pincet, Low energy cost for optimal speed and control of membrane fusion. *Proc. Natl. Acad. Sci. U.S.A.* **114**, 1238–1241 (2017).
5. F. Manca *et al.*, SNARE machinery is optimized for ultrafast fusion. *Proc. Natl. Acad. Sci. U.S.A.* **116**, 2435–2442 (2019).
6. A. Radhakrishnan *et al.*, Symmetrical arrangement of proteins under release-ready vesicles in presynaptic terminals. *Proc. Natl. Acad. Sci. U.S.A.* **118**, e2024029118 (2021).
7. X. Li *et al.*, Symmetrical organization of proteins under docked synaptic vesicles. *FEBS Lett.* **593**, 144–153 (2019).
8. J. Wang *et al.*, Calcium sensitive ring-like oligomers formed by synaptotagmin. *Proc. Natl. Acad. Sci. U.S.A.* **111**, 13966–13971 (2014).
9. O. D. Bello *et al.*, Synaptotagmin oligomerization is essential for calcium control of regulated exocytosis. *Proc. Natl. Acad. Sci. U.S.A.* **115**, E7624–E7631 (2018).
10. C. Ma, W. Li, Y. Xu, J. Rizo, Munc13 mediates the transition from the closed syntaxin-Munc18 complex to the SNARE complex. *Nat. Struct. Mol. Biol.* **18**, 542–549 (2011).
11. R. V. Kalyana Sundaram *et al.*, Munc13 binds and recruits SNAP25 to chaperone SNARE complex assembly. *FEBS Lett.* **595**, 297–309 (2021).
12. C. Ma, L. Su, A. B. Seven, Y. Xu, J. Rizo, Reconstitution of the vital functions of Munc18 and Munc13 in neurotransmitter release. *Science* **339**, 421–425 (2013).
13. X. Yang *et al.*, Syntaxin opening by the MUN domain underlies the function of Munc13 in synaptic-vesicle priming. *Nat. Struct. Mol. Biol.* **22**, 547–554 (2015).
14. K. Grushin, R. V. Kalyana Sundaram, C. V. Sindelar, J. E. Rothman, Munc13 structural transitions and oligomers that may choreograph successive stages in vesicle priming for neurotransmitter release. *Proc. Natl. Acad. Sci. U.S.A.* **119**, e2121259119 (2022).
15. J. E. Rothman, S. S. Krishnakumar, K. Grushin, F. Pincet, Hypothesis–Buttressed rings assemble, clamp, and release SNAREpins for synaptic transmission. *FEBS Lett.* **591**, 3459–3480 (2017).
16. N. Calakos, R. H. Scheller, Vesicle-associated membrane protein and synaptophysin are associated on the synaptic vesicle. *J. Biol. Chem.* **269**, 24534–24537 (1994).
17. A. Becher *et al.*, The synaptophysin-synaptobrevin complex: A hallmark of synaptic vesicle maturation. *J. Neurosci.* **19**, 1922–1931 (1999).
18. L. Edelmann, P. I. Hanson, E. R. Chapman, R. Jahn, Synaptobrevin binding to synaptophysin: A potential mechanism for controlling the exocytotic fusion machine. *EMBO J.* **14**, 224–231 (1995).
19. L. Thomas *et al.*, Identification of synaptophysin as a hexameric channel protein of the synaptic vesicle membrane. *Science* **242**, 1050–1053 (1988).
20. C. P. Arthur, M. H. Stowell, Structure of synaptophysin: A hexameric MARVEL-domain channel protein. *Structure* **15**, 707–714 (2007).
21. D. J. Adams, C. P. Arthur, M. H. Stowell, Architecture of the synaptophysin/synaptobrevin complex: Structural evidence for an entropic clustering function at the synapse. *Sci. Rep.* **5**, 13659 (2015).
22. D. N. White, M. H. B. Stowell, Room for two: The synaptophysin/synaptobrevin complex. *Front. Synaptic Neurosci.* **13**, 740318 (2021).
23. T. Sollner *et al.*, SNAP receptors implicated in vesicle targeting and fusion. *Nature* **362**, 318–324 (1993).
24. T. Weber *et al.*, SNAREpins: Minimal machinery for membrane fusion. *Cell* **92**, 759–772 (1998).
25. T. Sollner, M. K. Bennett, S. W. Whiteheart, R. H. Scheller, J. E. Rothman, A protein assembly-disassembly pathway in vitro that may correspond to sequential steps of synaptic vesicle docking, activation, and fusion. *Cell* **75**, 409–418 (1993).
26. V. Malhotra, L. Orci, B. S. Glick, M. R. Block, J. E. Rothman, Role of an N-ethylmaleimide-sensitive transport component in promoting fusion of transport vesicles with cisternae of the Golgi stack. *Cell* **54**, 221–227 (1988).
27. W. S. Trimble, D. M. Cowan, R. H. Scheller, VAMP-1: A synaptic vesicle-associated integral membrane protein. *Proc. Natl. Acad. Sci. U.S.A.* **85**, 4538–4542 (1988).
28. H. Sakamoto *et al.*, Synaptic weight set by Munc13-1 supramolecular assemblies. *Nat. Neurosci.* **21**, 41–49 (2018).
29. M. Bera, S. Ramakrishnan, J. Coleman, S. S. Krishnakumar, J. E. Rothman, Molecular determinants of complexin clamping and activation function. *Elife* **11**, e71938 (2022).
30. S. Ramakrishnan *et al.*, High-throughput monitoring of single vesicle fusion using freestanding membranes and automated analysis. *Langmuir* **34**, 5849–5859 (2018).
31. C. G. Giraudo, W. S. Eng, T. J. Melia, J. E. Rothman, A clamping mechanism involved in SNARE-dependent exocytosis. *Science* **313**, 676–680 (2006).
32. T. J. Melia *et al.*, Regulation of membrane fusion by the membrane-proximal coil of the t-SNARE during zippering of SNAREpins. *J. Cell Biol.* **158**, 929–940 (2002).
33. J. W. Kuhlmann, M. Junius, U. Diederichsen, C. Steinem, SNARE-mediated single-vesicle fusion events with supported and freestanding lipid membranes. *Biophys. J.* **112**, 2348–2356 (2017).
34. S. Ramakrishnan, M. Bera, J. Coleman, J. E. Rothman, S. S. Krishnakumar, Synergistic roles of Synaptotagmin-1 and complexin in calcium-regulated neuronal exocytosis. *Elife* **9**, e54506 (2020).
35. S. Ramakrishnan *et al.*, Synaptotagmin oligomers are necessary and can be sufficient to form a Ca(2+) -sensitive fusion clamp. *FEBS Lett.* **593**, 154–162 (2019).
36. K. P. Stepien, J. Rizo, Synaptotagmin-1-, Munc18-1-, and Munc13-1-dependent liposome fusion with a few neuronal SNAREs. *Proc. Natl. Acad. Sci. U.S.A.* **118** (2021).
37. K. P. Stepien, J. Xu, X. Zhang, X. C. Bai, J. Rizo, SNARE assembly enlightened by cryo-EM structures of a synaptobrevin–Munc18-1–syntaxin-1 complex. *Sci. Adv.* **8**, eabo5272 (2022).
38. X. Wang *et al.*, Munc13 activates the Munc18-1/syntaxin-1 complex and enables Munc18-1 to prime SNARE assembly. *EMBO J.* **39**, e103631 (2020).
39. R. V. Kalyana Sundaram *et al.*, Native planar asymmetric suspended membrane for single-molecule investigations: Plasma membrane on a chip. *Small* **18**, e2205567 (2022).
40. B. P. Ziemba, J. J. Falke, Lateral diffusion of peripheral membrane proteins on supported lipid bilayers is controlled by the additive frictional drags of (1) bound lipids and (2) protein domains penetrating into the bilayer hydrocarbon core. *Chem. Phys. Lipids* **172**, 67–77 (2013).
41. K. Glasmastar, C. Larsson, F. Hook, B. Kasemo, Protein adsorption on supported phospholipid bilayers. *J. Colloid Interface Sci.* **246**, 40–47 (2002).
42. C. Thiele, M. J. Hannah, F. Fahrenholz, W. B. Huttner, Cholesterol binds to synaptophysin and is required for biogenesis of synaptic vesicles. *Nat. Cell Biol.* **2**, 42–49 (2000).
43. J. Tong, P. P. Borbat, J. H. Freed, Y. K. Shin, A scissors mechanism for stimulation of SNARE-mediated lipid mixing by cholesterol. *Proc. Natl. Acad. Sci. U.S.A.* **106**, 5141–5146 (2009).
44. B. Seantier, B. Kasemo, Influence of mono- and divalent ions on the formation of supported phospholipid bilayers via vesicle adsorption. *Langmuir* **25**, 5767–5772 (2009).
45. P. S. Cremer, S. G. Boxer, Formation and spreading of lipid bilayers on planar glass supports. *J. Phys. Chem. B* **103**, 2554–2559 (1999).
46. S. Takamori *et al.*, Molecular anatomy of a trafficking organelle. *Cell* **127**, 831–846 (2006).
47. J. Zivanov *et al.*, New tools for automated high-resolution cryo-EM structure determination in RELION-3. *Elife* **7**, e42166 (2018).
48. X. Chen *et al.*, Three-dimensional structure of the complexin/SNARE complex. *Neuron* **33**, 397–409 (2002).
49. H. T. McMahon, M. Missler, C. Li, T. C. Sudhof, Complexins: Cytosolic proteins that regulate SNAP receptor function. *Cell* **83**, 111–119 (1995).
50. S. Pabst *et al.*, Rapid and selective binding to the synaptic SNARE complex suggests a modulatory role of complexins in neuroexocytosis. *J. Biol. Chem.* **277**, 7838–7848 (2002).
51. S. S. Krishnakumar *et al.*, Re-visiting the trans insertion model for complexin clamping. *Elife* **4**, e04463 (2015).
52. F. Li *et al.*, A half-zippered SNARE complex represents a functional intermediate in membrane fusion. *J. Am. Chem. Soc.* **136**, 3456–3464 (2014).
53. D. Kummel *et al.*, Complexin cross-links prefusion SNAREs into a zigzag array. *Nat. Struct. Mol. Biol.* **18**, 927–933 (2011).
54. A. Bracher, J. Kadlec, H. Betz, W. Weissenhorn, X-ray structure of a neuronal complexin-SNARE complex from squid. *J. Biol. Chem.* **277**, 26517–26523 (2002).
55. J. Malsam *et al.*, Complexin suppresses spontaneous exocytosis by capturing the membrane-proximal regions of VAMP2 and SNAP25. *Cell Rep.* **32**, 107926 (2020).
56. R. W. Cho *et al.*, Genetic analysis of the Complexin trans-clamping model for cross-linking SNARE complexes in vivo. *Proc. Natl. Acad. Sci. U.S.A.* **111**, 10317–10322 (2014).
57. J. Gong *et al.*, C-terminal domain of mammalian complexin-1 localizes to highly curved membranes. *Proc. Natl. Acad. Sci. U.S.A.* **113**, E7590–E7599 (2016).
58. D. Snead, R. T. Wragg, J. S. Dittman, D. Eliezer, Membrane curvature sensing by the C-terminal domain of complexin. *Nat. Commun.* **5**, 4955 (2014).
59. B. G. Wilhelm *et al.*, Composition of isolated synaptic boutons reveals the amounts of vesicle trafficking proteins. *Science* **344**, 1023–1028 (2014).
60. R. Laage, D. Langosch, Dimerization of the synaptic vesicle protein synaptobrevin (vesicle-associated membrane protein) II depends on specific residues within the transmembrane segment. *Eur. J. Biochem.* **249**, 540–546 (1997).
61. S. Wittig *et al.*, Oligomerisation of Synaptobrevin-2 studied by native mass spectrometry and chemical cross-linking. *J. Am. Soc. Mass Spectrom.* **30**, 149–160 (2019).
62. A. Panda *et al.*, Direct determination of oligomeric organization of integral membrane proteins and lipids from intact customizable bilayer. *Nat. Methods* **20**, 891–897 (2023).
63. Y. T. Hsiao, M. B. Jackson, Synaptophysin transmembrane domain III controls fusion pore dynamics in Ca(2+)-triggered exocytosis *Biophys. J.* **122**, 1962–1973 (2023).
64. J. E. Rothman, K. Grushin, M. Bera, F. Pincet, Turbocharging synaptic transmission. *FEBS Lett.* **597**, 2233–2249 (2023).
65. S. Wang *et al.*, Munc18 and Munc13 serve as a functional template to orchestrate neuronal SNARE complex assembly. *Nat. Commun.* **10**, 69 (2019).
66. M. K. Raja *et al.*, Elevated synaptic vesicle release probability in synaptophysin/gyrin family quadruple knockouts. *Elife* **8**, e40744 (2019).
67. S. L. Gordon, R. E. Leube, M. A. Cousin, Synaptophysin is required for synaptobrevin retrieval during synaptic vesicle endocytosis. *J. Neurosci.* **31**, 14032–14036 (2011).
68. S. E. Kwon, E. R. Chapman, Synaptophysin regulates the kinetics of synaptic vesicle endocytosis in central neurons. *Neuron* **70**, 847–854 (2011).
69. L. K. Mahal, S. M. Sequeira, J. M. Gureasko, T. H. Sollner, Calcium-independent stimulation of membrane fusion and SNAREpin formation by synaptotagmin I. *J. Cell Biol.* **158**, 273–282 (2002).
70. S. Ahmed, M. Holt, D. Riedel, R. Jahn, Small-scale isolation of synaptic vesicles from mammalian brain. *Nat. Protoc.* **8**, 998–1009 (2013).
71. D. N. Mastronarde, Automated electron microscope tomography using robust prediction of specimen movements. *J. Struct. Biol.* **152**, 36–51 (2005).
72. S. Q. Zheng *et al.*, MotionCor2: Anisotropic correction of beam-induced motion for improved cryo-electron microscopy. *Nat. Methods* **14**, 331–332 (2017).
73. A. Rohou, N. Grigorieff, CTFFIND4: Fast and accurate defocus estimation from electron micrographs. *J. Struct. Biol.* **192**, 216–221 (2015).